Hindawi
Advances in Materials Science and Engineering
Volume 2018, Article ID 2809356, 8 pages
https://doi.org/10.1155/2018/2809356

Research Article

Microstructures and Mechanical Properties of Al/Fe and Cu/Fe Joints by Continuous Drive Friction Welding

Yanni Wei[1] **and Fu Sun**[2]

[1]*Department of Materials Science and Engineering, Xi'an University of Technology, 5 South Jinhua Road, Xi'an 710048, China*
[2]*Shaanxi Zhituo Solid-State Additive Manufacturing Technology Company, 70 West of Chaoyang Street, Weinan 714000, China*

Correspondence should be addressed to Yanni Wei; weiyanni@xaut.edu.cn

Received 2 April 2018; Revised 19 May 2018; Accepted 28 May 2018; Published 27 June 2018

Academic Editor: Paolo Ferro

The dissimilar pure metals Al/Fe and Cu/Fe with different metallurgical compatibility were joined by continuous drive friction welding. The friction weldability was investigated. The microstructure of the joining interface was analyzed by scanning electron microscopy, and the chemical compositions were tested by energy-dispersive spectroscopy. The joining strength was evaluated by tensile test, and the fracture was detected by X-ray diffraction analysis. The results show that sound joints of Al/Fe and Cu/Fe can be obtained by continuous drive friction welding process. A discontinuous reaction layer was formed on Al/Fe interface, and no obvious reaction layer appeared on Cu/Fe interface. The tensile strength of the joints increased with increasing friction pressure, and the highest strength could reach up to 70 MPa for Al/Fe joint and 222 MPa for Cu/Fe joint. All the Al/Fe friction-welded samples failed at the friction interface, while the Cu/Fe joint under 36 and 44 MPa friction pressure failed at Cu matrix during the tensile test.

1. Introduction

The need for joints between dissimilar materials often arises in extensive industrial applications [1]. A sound joining technique can provide interesting combinations of structural and functional properties, which can offer many benefits [2]. As widely used materials, aluminum/steel structure can obviously reduce weight, and copper/steel structure can provide effectively combinations of conductivity and strength [3, 4]. Welding process is the key technology to manufacture the dissimilar materials composite structures. But it is difficult to use the traditional fusion welding method because of the tremendous difference in mechanical and metallurgical properties between dissimilar materials [5]. Continuous drive friction welding (CDFW), as the most promising method to join dissimilar materials, is importantly demanded in the manufacture of a new generation of aircraft, rocket, and shipboard equipment because of the advantages such as high material savings and low production time [6–8].

CDFW is a solid-state joining method that utilizes friction-induced thermomechanical deformation to create high-quality welds. In previous works, dissimilar metals such as Al/Fe [6, 7], Al/Ti [8], Al/Cu [9], Cu/Fe [4], Ti/Fe [10], and Cu/alumina ceramic [11] of the friction welding have been carried out by many researchers. In particularly, aluminum/steel [7] and copper/steel [12] friction welding joints present good performance with tensile strength higher than the matrix. It is generally known that the excellent mechanical property of the friction welding joint is due to its reliable metallurgical bonding quality and microstructure characteristics of ultrafine crystals and even nanocrystals [13]. During the joint formation, the materials near the interface of dissimilar metal have simultaneously encountered high temperature and severe plastic deformation. The metallurgical interactions on the dissimilar interface are critical for the joint strength and stability, which attract a lot of attention by researchers [14, 15]. Correlational studies were mainly the analysis of the relationship between the parameters and the joint microstructures and performance [16].

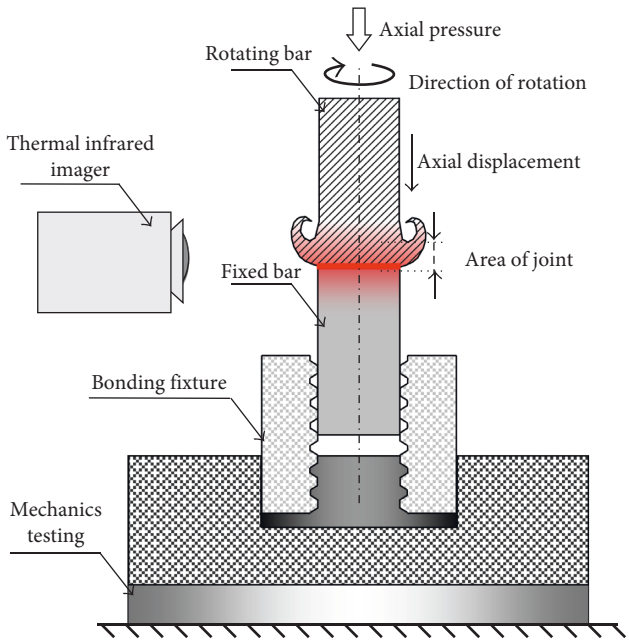

Figure 1: Schematic diagram of continuous drive friction welding.

However, the metallurgical compatibility between the dissimilar metals and its influence on joint microstructure evolution have not been clarified.

In this paper, the dissimilar pure metals Al/Fe and Cu/Fe with different metallurgical compatibility were designed, and a physical simulation apparatus of rotation friction welding was used to investigate the friction weldability. The microstructures of the joining interface were analyzed by scanning electron microscopy (SEM) with EDS, the joining strength was evaluated by tensile test, and the fracture was tested by X-ray diffraction analysis. The microhardness of the interface region was tested.

2. Experimentation Procedure

Commercially available bars of Al (99.6 wt.%), Cu (99.9 wt.%), and Fe (99.95 wt.%) were used. The specimens were machined with a dimension of 20 mm in the joining part and 14 mm in the clamping part. Before joining, the specimens' surfaces were milled and degreased with acetone. The experimental schematic is shown in Figure 1. Before welding, the rotating bar was rotated around its axis while the fixed bar was irrotational. When the rotation speed reached the preestablished parameter, the fixed bar moved along the axis and then contacted with the rotating bar under the action of hydraulic pressure, and then, the friction process began. The rotation speeds were 1200 rpm for Al/Fe and 1900 rpm for Cu/Fe couples. The different axial pressure was used as 20, 28, 36, 44 MPa, with friction time 5 s. In the meanwhile, the interface temperature was observed using an infrared thermographic imager (InfraTec, VarioCAM®hr head-HS) with the frame rate of 60 fps and thermocouple synchronously.

After joining, the welded sample for metallographic examination was cut perpendicular to the welding interface. The samples were subjected to metallographic characterization employing scanning electron microscopy (SEM, JEOL, JSM-6700) equipped with an energy-dispersive spectrum (EDS) and transmission electron microscope (TEM, JEM-3010). The mechanical properties of the joints were evaluated by tensile tests (Instron 5880) at a constant displacement rate of 1 mm/min at room temperature. The microhardness of the interface region was measured by the microhardness tester.

3. Results and Discussion

3.1. Joints Appearance and the Burn-Off Length. Figure 2 shows the appearance of the welded joints with different friction pressure. It is evident that the upset metal of the welded Al/Fe and Cu/Fe joints increases gradually with the friction pressure being increased. During the CDFW process, the accumulated friction heat is sufficient to soften the matrix. The upset metal subsequently forms under the squeezing action of friction pressure when the matrix reaches the plastic state. The deformation mainly occurs in Al side for Al/Fe joints and Cu side for Cu/Fe joints. The burn-off length increases with the increase of friction pressure in both joints, as shown in Table 1.

3.2. The Interface Temperature. During the CDFW process, the temperature of the interface region was detected by the thermal infrared imager and the thermocouple embedded in the fixed bar 1.5 mm from the interface simultaneously. The test results are shown in Figure 3. Figure 3(a) is a typical infrared thermal image of the welding interface, and Figure 3(b) shows the temperature changes over time during the whole welding process by the thermocouple. The area between two dashed lines in Figure 3(b) indicated the actual friction time. The temperature curves show an unsteady ascent stage and then attain a relatively stable stage which shows that the heat production and exothermic reaction reach equilibrium. The average temperatures of this equilibrium state were regarded as the welding temperature. The welding temperatures of both Al/Fe and Cu/Fe joints increase with the increase of the welding pressure.

3.3. Microstructure of Joints. The defect-free joints were obtained by the continuous drive friction welding experiments. The typical interface morphology of Al/Fe and Cu/Fe CDFW joints is shown in Figure 4. The Al/Fe interface formed a discontinuous reaction layer when the gray scale was between Al and Fe, as shown in Figure 4(a). Fe side near the interface presented relatively flat, and the reaction products were all embedded in the Al matrix. The Cu/Fe interface presented good bonding although no obvious reaction layer appeared which is shown in Figure 4(b). It showed good deformation coordination on both sides of the interface because of the similar elastic modulus between pure Cu and Fe metals. The elementary compositions on the interface region were tested by energy-dispersive X-ray spectroscopy (EDS) analysis of the interface. The EDS results for different regions in Figure 4 are shown in Table 2.

(a) (b)

Figure 2: Appearance of (a) Al/Fe and (b) Cu/Fe joints at different welding pressure.

Table 1: Friction welding parameters in the experiments and the burn-off length of joints.

Dissimilar joint	Friction pressure (MPa)	Rotation speeds (rpm)	Burn-off (mm)
Al/Fe	20	1200	2.1
	28		4.4
	36		5.4
	44		8.3
Cu/Fe	20	1900	2.9
	28		4.5
	36		6.4
	44		11.5

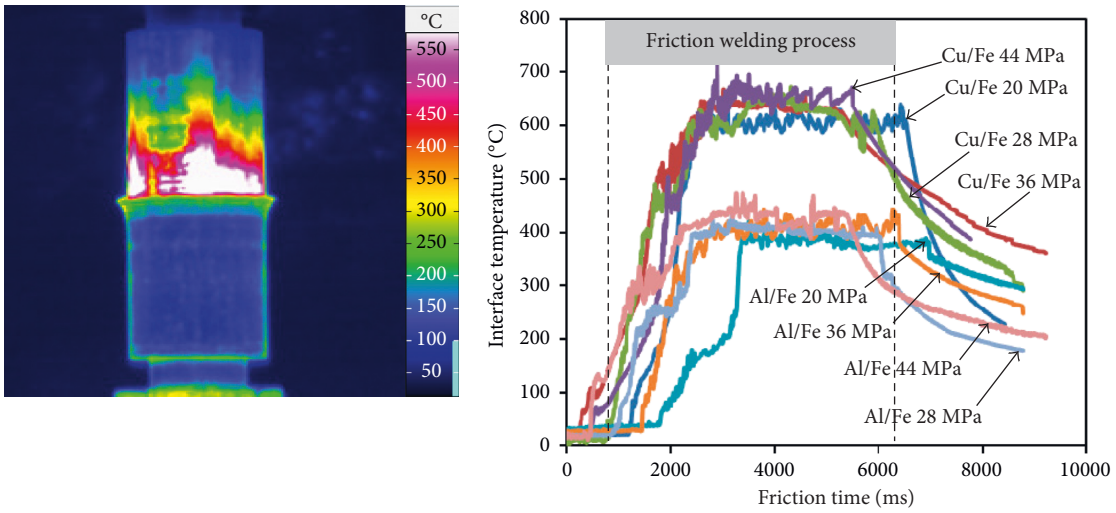

(a) (b)

Figure 3: The interface temperature during the CDFW process shown as (a) temperature pattern by thermal infrared imager and (b) temperature variation curve by thermocouple.

The molar ratio of Al to Fe in the reaction layer (points 01 and 02) is 3 : 1 approximately, and it could be speculated that this might be the Al_3Fe intermetallic. The region of point 03 is the Fe matrix. The compositions of the region points 04 and 05 indicated the metallurgical bonding occurred on the Cu/Fe joint. It might be nonequilibrium solid solution in region point 04 and possible phase $FeCu_4$ in region point 05.

Figure 5 shows the micromorphology of the Al/Fe joining interfaces under different welding pressure. There was no reaction product on the interface when the welding pressure was 20 MPa as shown in Figure 5(a). The amount of

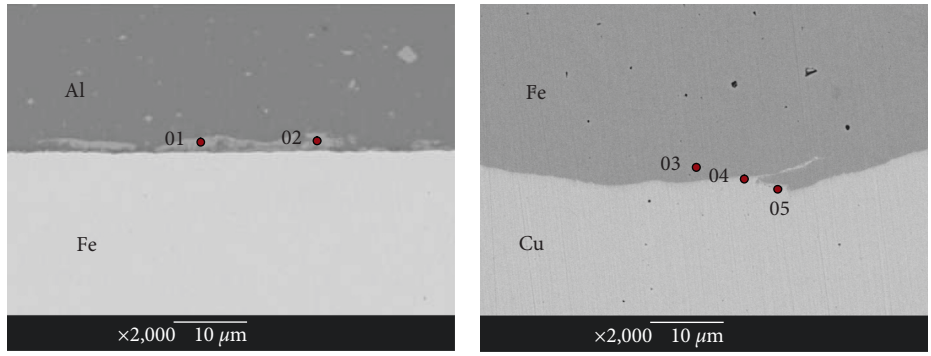

Figure 4: The typical interface morphology: (a) Al/Fe interface and (b) Cu/Fe interface.

Table 2: Composition analyses of the points indicated in Figure 4 (at.%).

Test positions	Al	Fe	Cu	O	Possible phase
01	73.78	24.02	—	2.20	Al_3Fe
02	75.67	23.58	—	0.75	Al_3Fe
03	—	99.94	—	0.06	Fe matrix
04	—	72.21	25.34	2.45	Solid solution
05	—	20.13	78.27	1.60	$FeCu_4$

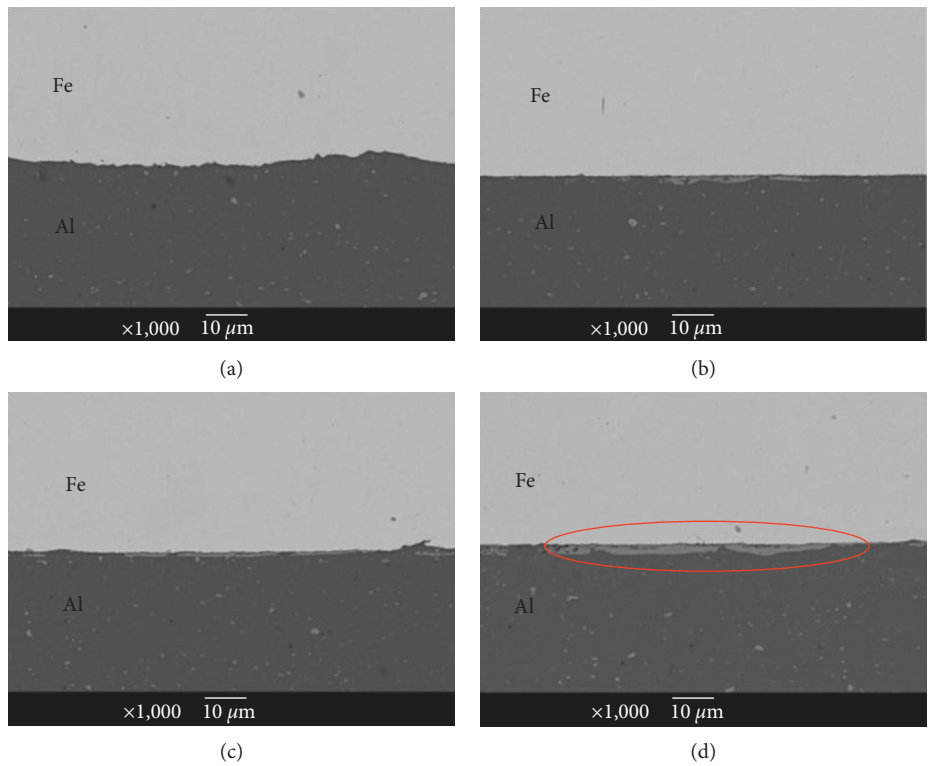

Figure 5: Microstructures of Al/Fe welding region metallurgical reaction layer under: (a) 20; (b) 28; (c) 36; (d) 44 MPa.

the reaction product increases with the increase of welding pressure (Figures 5(b)–5(d)). The reaction layer presented discontinuous distribution and uneven thickness characteristics. The thickest region reached 4 μm.

There was no visible difference in the morphology of the Cu/Fe joining interfaces under different welding pressure. Thus, the detailed microstructures of the interfacial region on the Cu/Fe joining interface were detected. Figure 6 shows the

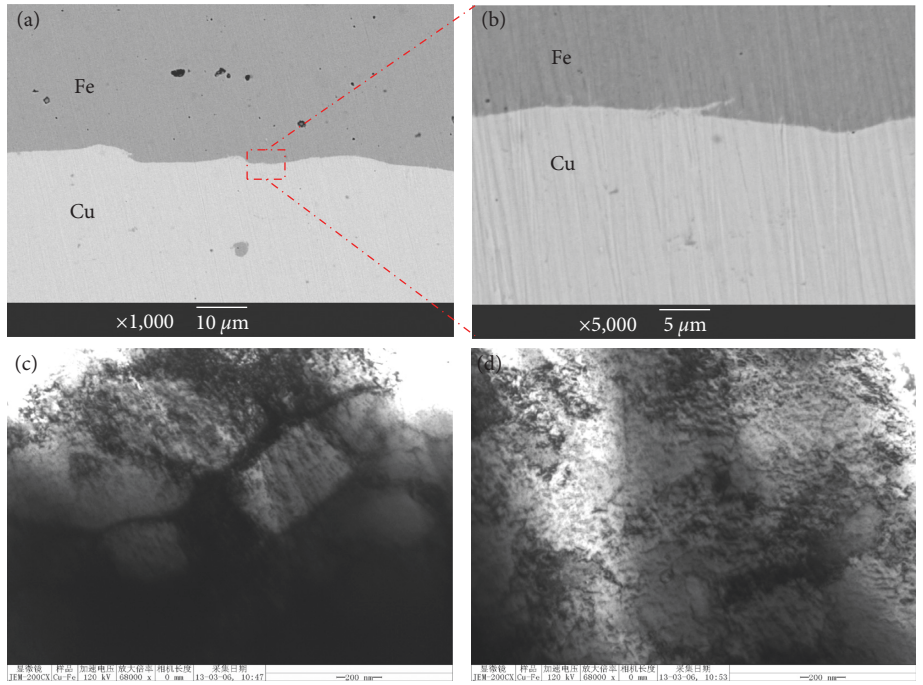

Figure 6: The typical interface morphology of the Cu/Fe interface shown as (a, b) SEM images, (c) TEM image of welding interface, and (d) dislocation line.

typical micromorphology of the Cu/Fe joining interface under 36 MPa welding pressure. The images of larger magnification (shown in Figure 6(b)) presented gradient transition characteristics in gray scale with different element content.

Further analysis obtained by TEM shows better solution on Cu/Fe joining interface as shown in Figure 6(c). This indicated that the mutual diffusion between Cu and Fe occurred though Cu–Fe was an immiscible system in thermodynamic equilibrium state. Figure 6(d) shows the high-density dislocation in severe deformed Cu matrix near the interface. For forced mixing, alloy components are thus assumed to flow down gradients in their concentrations, while for thermally activated diffusion atoms flow down gradients in their chemical potentials. So, the diffusion in immiscible Cu/Fe couples was most attributed to the forced mixing along the concentration gradient.

3.4. Mechanical Properties of the Joints. Figure 7 shows the tensile strength of the Al/Fe and Cu/Fe joints as a function of the welding pressure. It can be found that the tensile strength increases along with the welding pressure and reaches a maximum value as 70 MPa for Al/Fe joint and 222 MPa for Cu/Fe joint. The dashed lines in Figure 7 denote the tensile strength of Al matrix with 88 MPa and Cu matrix with 218 MPa obtained by a tensile test. Such result implies that joining strength of Cu/Fe CDFW joints falls around that of the Cu matrix at the welding pressure of 36 MPa and the ultimate fracture happens at Cu matrix. The results indicated that the sound joint with defect-free interface microstructure and excellent joint strength was obtained for Cu/Fe dissimilar metals. However, the maximum joining strength of Al/Fe CDFW joints was slightly lower than that of Al matrix.

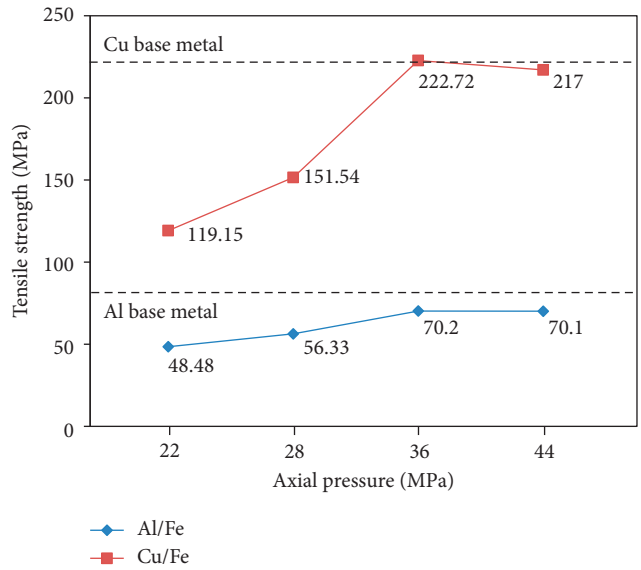

Figure 7: The tensile strength of the Al/Fe and Cu/Fe joints as a function of welding pressure.

This might be due to the existence of the discontinuous reaction layer and the differences of Young's modulus between Al and Fe. All the joints were fractured at the Al/Fe interface. Figure 8 shows the representative stress-strain curve of the Al/Fe and Cu/Fe joints during the tensile test.

The microhardness across the interface of the Al/Fe and Cu/Fe joints was tested. The interface microhardness distributions of different joints are shown in Figure 9. The hardness value increased near the interface. This is mainly due to grain refinement in the deformation area.

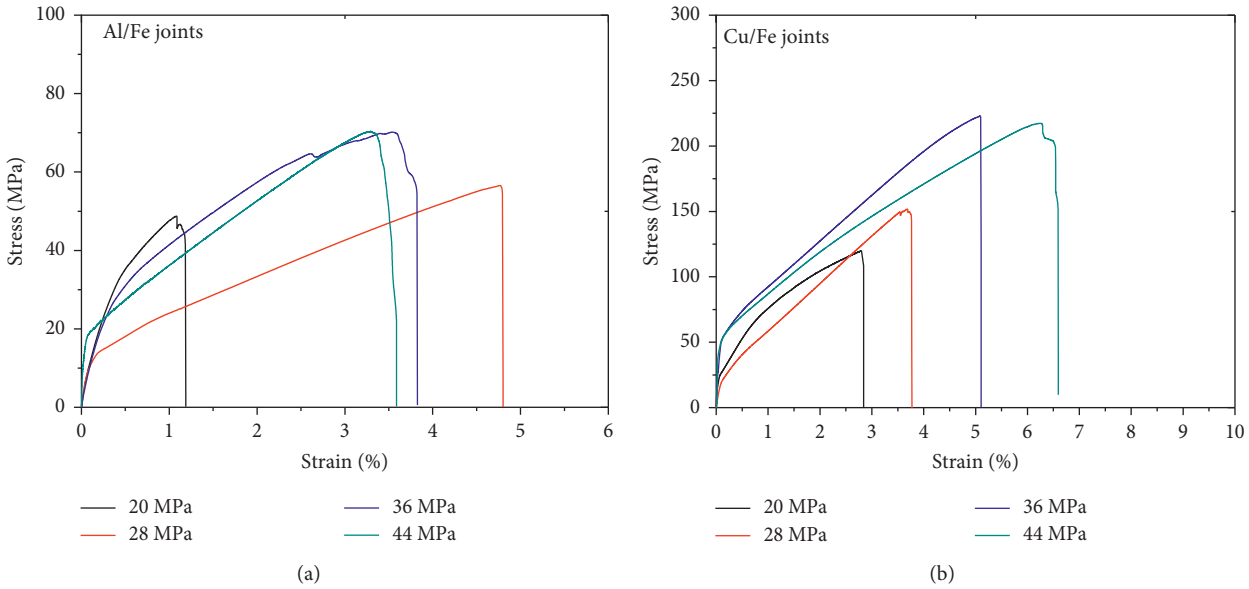

Figure 8: The representative stress-strain curve of the Al/Fe and Cu/Fe joints during the tensile test.

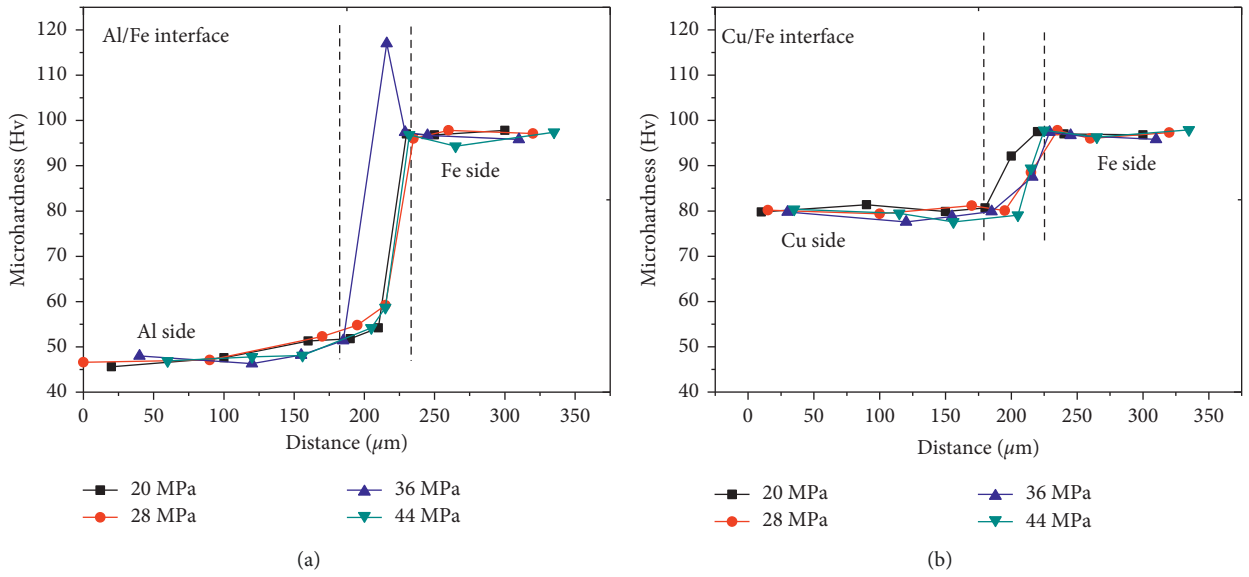

Figure 9: The interface microhardness distributions of different joints: (a) Al/Fe interface and (b) Cu/Fe interface.

3.5. Fracture Morphology and Phase Analysis. Figure 10 shows the XRD phase analysis and morphologies of the fractured surfaces of the Al/Fe joints. The XRD phase analysis result indicated that there was small amount of Fe on the Al side fractured surfaces and small amount of Al on the Fe side fractured surfaces. There are no obvious peaks of intermetallic compounds. Figures 10(b) and 10(c) show the morphologies of the Al side and Fe side fractured surfaces of the Al/Fe joint. It can be seen that the morphologies of Al side fractured surfaces showed some gap ups and downs. However, the morphologies of Fe side were mainly the flat region partially covered by a mixed layer.

Figure 11 shows the XRD phase analysis and morphologies of the fractured surfaces of the Cu/Fe joints. It can be found that there was only Cu phase on the fractured surfaces of Cu side, while Fe, Cu, and $FeCu_4$ on the fractured surfaces of Fe side, as shown in Figure 11(a). Figure 11(b) shows the morphologies of the Cu side fractured surfaces of the Cu/Fe joint. It was a typical ductile fracture of Cu matrix. Figure 11(c) shows the morphologies of the Fe side fractured surfaces of the Cu/Fe joint. Some small particles appeared in the vortices. The result indicated that the sample was fractured in Cu matrix near the interface. Then, the tensile strength was close to Cu metal. There was a small amount of $FeCu_4$ intermetallic compounds formed on the interface. The solid solubility of Cu and Fe element was achieved on the interface.

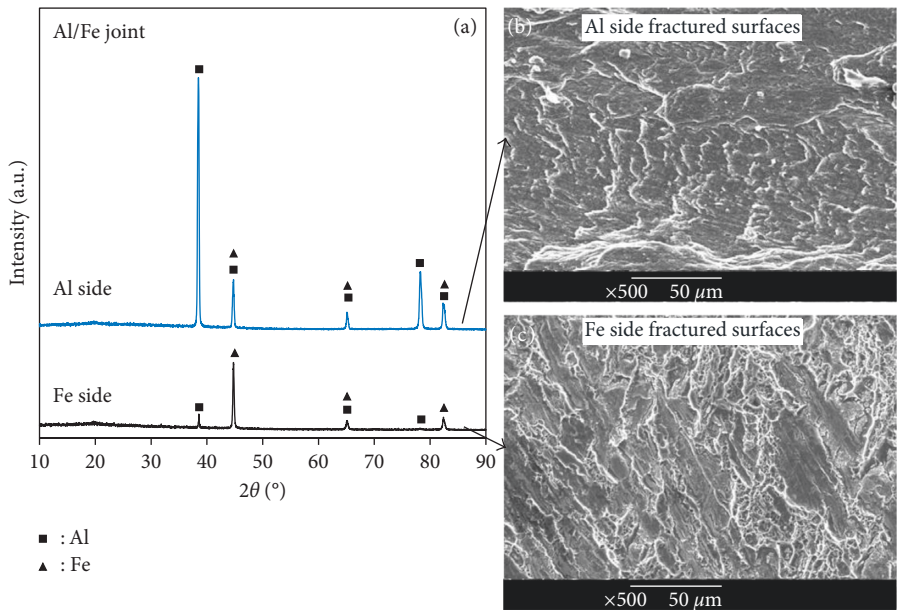

Figure 10: XRD phase analysis and morphologies of the fractured surfaces of the Al/Fe joints.

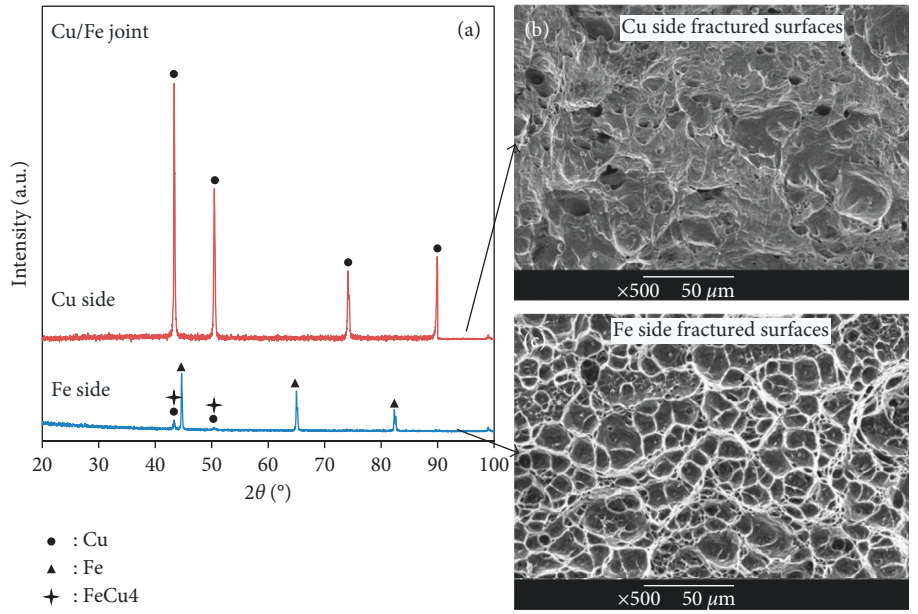

Figure 11: XRD phase analysis and morphologies of the fractured surfaces of the Cu/Fe joints.

4. Conclusions

The dissimilar pure metals Al/Fe and Cu/Fe with different metallurgical compatibility were joined by continuous drive friction welding. The microstructure of the joining interface was analyzed, the joining strength was evaluated by tensile shear test, and the fracture was tested by X-ray diffraction analysis. The main conclusions are as follows:

(1) The sound joints of Al/Fe and Cu/Fe can be obtained by continuous drive friction welding process. A discontinuous reaction layer was formed on Al/Fe friction interface and no obvious reaction layer appeared on Cu/Fe interface.

(2) The tensile strength of the joints increased with increasing friction pressure, and the highest strength could reach up to 70 MPa for Al/Fe joint and 222 MPa for Cu/Fe joint. All the Al/Fe friction-welded samples failed at the friction interface, while the Cu/Fe joint under 36 and 44 MPa friction pressures failed at Cu matrix during tensile test.

Data Availability

All data generated or analysed during this study are included within the article.

Conflicts of Interest

The authors declare that they have no conflicts of interest.

Acknowledgments

This work is financially supported by the National Natural Science Foundation of China under Grant no. 51701154, the Key Research and Development Project of Shaanxi Province under Grant no. 2017ZDXM-GY-033, the China Postdoctoral Science Foundation-Funded Project under Grant no. 2016M592823, the Scientific Research Project of Shaanxi Provincial Department of Education under Grant no. 17JK0563, and the Scientific Research Foundation of Xian University of Technology under Grant no. 101-451115015.

References

[1] W. Guo, G. Q. You, G. Y. Yuan, and X. L. Zhang, "Microstructure and mechanical properties of dissimilar inertia friction welding of 7A04 aluminum alloy to AZ31 magnesium alloy," *Journal of Alloys and Compounds*, vol. 695, pp. 3267–3277, 2017.

[2] A. Yazdipourn and A. Heidarzadeh, "Effect of friction stir welding on microstructure and mechanical properties of dissimilar Al 5083-H321 and 316L stainless steel alloy joints," *Journal of Alloys and Compounds*, vol. 680, pp. 595–603, 2016.

[3] Y. Kusuda, "Honda develops robotized FSW technology to weld steel and aluminum and applied it to a mass production vehicle," *Industrial Robot: An International Journal*, vol. 40, pp. 208–212, 2013.

[4] M. Sahin, E. Cil, and C. Misirli, "Characterization of properties in friction welded stainless steel and copper materials," *Journal of Materials Engineering and Performance*, vol. 22, no. 3, pp. 840–847, 2013.

[5] Y. N. Wei, J. L. Li, J. T. Xiong, F. Huang, F. S. Zhang, and S. H. Raza, "Joining aluminum to titanium alloy by friction stir lap welding with cutting pin," *Materials Characterization*, vol. 71, pp. 1–5, 2012.

[6] A. Ambroziak, M. Korzeniowski, P. KustroN, M. Winnicki, P. SokoBowski, and E. HarapiNska, "Friction welding of aluminium and aluminium alloys with steel," *Advances in Materials Science and Engineering*, vol. 2014, Article ID 981653, 15 pages, 2014.

[7] M. Kimura, M. Kusaka, K. Kaizu, K. Nakata, and K. Nagatsuk, "Friction welding technique and joint properties of thin-walled pipe friction-welded joint between type 6063 aluminum alloy and AISI 304 austenitic stainless steel," *International Journal of Advanced Manufacturing Technology*, vol. 82, no. 1–4, pp. 489–499, 2016.

[8] M. Meisnar, S. Baker, J. M. Bennett et al., "Microstructural characterisation of rotary friction welded AA6082 and Ti-6Al-4V dissimilar joints," *Materials and Design*, vol. 132, pp. 188–197, 2017.

[9] M. N. Avettand-Fènoël, G. Racineux, L. Debeugny, and R. Taillard, "Microstructural characterization and mechanical performance of an AA2024 aluminium alloy—pure copper joint obtained by linear friction welding," *Materials and Design*, vol. 98, pp. 305–318, 2016.

[10] X. Li, J. L. Li, Z. X. Liao, F. Jin, F. S. Zhang, and J. T. Xiong, "Microstructure evolution and mechanical properties of rotary friction welded TC4/SUS321 joints at various rotation speeds," *Materials and Design*, vol. 99, pp. 26–36, 2016.

[11] P. Li, J. L. Li, H. G. Dong, and C. Z. Ji, "Metallurgical and mechanical properties of continuous drive friction welded copper/alumina dissimilar joints," *Materials and Design*, vol. 127, pp. 311–319, 2017.

[12] M. Kimura, M. Kusaka, K. Kaizu, and A. Fuji, "Effect of friction welding condition on joining phenomena and tensile strength of friction welded joint between pure copper and low carbon steel," *Journal of Solid Mechanics and Materials Engineering*, vol. 3, no. 2, pp. 187–198, 2009.

[13] R. Palanivel, I. Dinaharan, and R. F. Laubscher, "Assessment of microstructure and tensile behavior of continuous drive friction welded titanium tubes," *Materials Science and Engineering A*, vol. 687, pp. 249–258, 2017.

[14] Y. Morisada, T. Imaizumi, and H. Fujii, "Determination of strain rate in friction stir welding by three-dimensional visualization of material flow using X-ray radiography," *Scripta Materialia*, vol. 106, pp. 57–60, 2015.

[15] Y. N. Wei, J. T. Xiong, J. L. Li, F. S. Zhang, and S. H. Liang, "Microstructure and enhanced atomic diffusion of friction stir welding aluminium/steel joints," *Materials Science and Technology*, vol. 33, no. 10, pp. 1208–1214, 2017.

[16] M. Pourali, A. Abdollah-zadeh, T. Saeid, and F. Kargar, "Influence of welding parameters on intermetallic compounds formation in dissimilar steel/aluminum friction stir welds," *Journal of Alloys and Compounds*, vol. 715, pp. 1–8, 2017.